JOURNAL OF GEOPHYSICAL RESEARCH: ATMOSPHERES, VOL. 118, 9168–9181, doi:10.1002/jgrd.50617, 2013

Improvement of MODIS aerosol retrievals near clouds

Guoyong Wen,[1,2] Alexander Marshak,[2] Robert C. Levy,[2] Lorraine A. Remer,[3] Norman G. Loeb,[4] Tamás Várnai,[2,3] and Robert F. Cahalan[2]

Received 31 December 2012; revised 26 June 2013; accepted 28 June 2013; published 28 August 2013.

[1] The retrieval of aerosol properties near clouds from reflected sunlight is challenging. Sunlight reflected from clouds can effectively enhance the reflectance in nearby clear regions. Ignoring cloud 3-D radiative effects can lead to large biases in aerosol retrievals, risking an incorrect interpretation of satellite observations on aerosol-cloud interaction. Earlier, we developed a simple model to compute the cloud-induced clear-sky radiance enhancement that is due to radiative interaction between boundary layer clouds and the molecular layer above. This paper focuses on the application and implementation of the correction algorithm. This is the first time that this method is being applied to a full Moderate Resolution Imaging Spectroradiometer (MODIS) granule. The process of the correction includes converting Clouds and the Earth's Radiant Energy System broadband flux to visible narrowband flux, computing the clear-sky radiance enhancement, and retrieving aerosol properties. We find that the correction leads to smaller values in aerosol optical depth (AOD), Ångström exponent, and the small mode aerosol fraction of the total AOD. It also makes the average aerosol particle size larger near clouds than far away from clouds, which is more realistic than the opposite behavior observed in operational retrievals. We discuss issues in the current correction method as well as our plans to validate the algorithm.

Citation: Wen, G., A. Marshak, R. C. Levy, L. A. Remer, N. G. Loeb, T. Várnai, and R. F. Cahalan (2013), Improvement of MODIS aerosol retrievals near clouds, *J. Geophys. Res. Atmos.*, *118*, 9168–9181, doi:10.1002/jgrd.50617.

1. Introduction

[2] Aerosols play a profound role in Earth's climate. The aerosol amount near clouds is an important parameter for studying aerosol radiative forcing, aerosol-cloud interactions, and cloud processes. A great deal of effort has been made to study aerosol properties in the vicinity of clouds [e.g., *Charlson et al*., 2007; *Koren et al*., 2007; *Su et al*., 2008; *Tackett and Di Girolamo*, 2009; *Varnai and Marshak*, 2011; *Redemann et al*., 2009; *Jeong and Li*, 2010]. They show that aerosol near clouds has very different characteristics in particle size and in optical properties linked to cloud processes. It is necessary to extend the research to further quantify aerosol radiative forcing, aerosol-cloud interactions, and impact of aerosol on climate on regional and global scales.

[3] Satellite observations provide a unique opportunity to study the role of aerosol in the climate system on regional and global scales. The Moderate Resolution Imaging Spectroradiometer (MODIS), an Earth Observing System (EOS) facility instrument, is well suited to observe the spatial and temporal characteristics of aerosol properties from space [*King et al*., 1992]. The MODIS operational one-dimensional (1-D) algorithm has provided valuable daily products of aerosol properties on a global scale over the past decade. However, the retrieval of aerosols near clouds using reflected sunlight is challenging. This is because the optical properties near clouds display strong three-dimensional (3-D) variations, and the radiative transfer process near clouds becomes very complicated. Sunlight reflected from clouds can effectively enhance the reflectance of clear regions nearby [e.g., *Wen et al*., 2008; *Kassianov and Ovtchinnikov*, 2008; *Marshak et al*., 2008]. Ignoring cloud 3-D radiative effects can lead to large errors in aerosol retrievals and incorrect interpretations of satellite observations on aerosol-cloud interaction.

[4] To isolate real aerosol variations near clouds, one must correct 3-D cloud radiative effects that are not accounted for in operational 1-D retrievals. Several methods have been developed for correcting 3-D cloud radiative effects on reflected solar radiation and aerosol retrievals in the vicinity of clouds [e.g., *Marshak et al*., 2008; *Kassianov and Ovtchinnikov*, 2008]. We have implemented our two-layer model [*Marshak et al*., 2008] to make it applicable to a full MODIS granule.

[5] In this paper we present details of the algorithm for correcting aerosol optical properties for the cloud 3-D radiative effects. Section 2 presents the methodology, and in section 3, we further perform consistency checks about the assumptions in the correction algorithm. The results are presented in section 4, followed by a summary and discussion of the results in the final section.

[1]GESTAR, Morgan State University, Baltimore, Maryland, USA.
[2]NASA Goddard Space Flight Center, Greenbelt, Maryland, USA.
[3]University of Maryland Baltimore County, Joint Center for Earth Systems Technology, USA.
[4]NASA Langley Research Center, Hampton, Virginia, USA.

Corresponding author: G. Wen, NASA Goddard Space Flight Center, Code 613, Greenbelt, MD 20771, USA. (Guoyong.Wen-1@nasa.gov)

2169-897X/13/10.1002/jgrd.50617

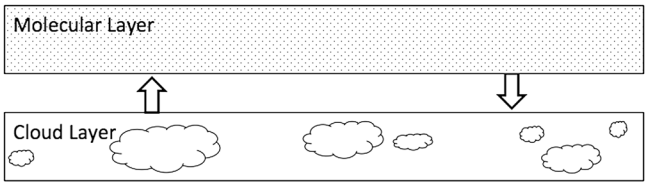

Figure 1. A sketch of the two-layer model similar to the one developed in *Marshak et al*. [2008] for deriving the radiative enhancement of clear-sky reflectance in a cloud field.

2. Method

[6] 3-D radiative transfer simulations demonstrate that scattering of sunlight by clouds, followed by upward Rayleigh scattering by air molecules above cloud top altitude over clear gaps, is a dominant mechanism for the enhancement of visible reflectance in clear regions in the case of boundary layer cumulus fields that lie over dark surfaces with aerosols trapped in the boundary layer [*Wen et al*., 2008]. A two-layer model has been developed to correct the clear-sky reflectance enhancement from cloud-molecular scattering [*Marshak et al*., 2008]. By using the corrected reflectances as input to the MODIS operational aerosol algorithm, one obtains corrected aerosol optical properties. Here we briefly describe the two-layer model for computing clear-sky reflectance enhancements and the steps for correcting aerosol properties.

2.1. The Two-Layer Model

[7] The two-layer model for computing the clear-sky reflectance enhancement due to clouds is presented in Figure 1. For a MODIS 10 km × 10 km grid box, the cloud-induced clear-sky reflectance enhancement can be estimated if the upward narrowband flux (or albedo) from the cloud layer is known. Having the narrowband upward flux from the cloud layer, one may compute the clear-sky reflectance enhancement (ΔR) using a slightly modified two-layer model [*Marshak et al*., 2008]. Similar to *Marshak et al*. [2008], we consider two radiances: (1) one is reflected from a broken cloud field with scattering Rayleigh layer above it and (2) one is reflected from the same broken cloud field but the molecules in the upper layer causing extinction, but no scattering.

$$R_1(\lambda,\Omega,\Omega_0) = R_m(\tau(\lambda),\Omega,\Omega_0) + \frac{\alpha_N(\lambda)T_m(\tau(\lambda),\Omega_0)}{1-\alpha_N(\lambda)R_{m,\mathrm{diff}}(\tau(\lambda))}T_{m,\mathrm{diff}}(\tau(\lambda),\Omega), \quad (1)$$

$$R_2(\lambda,\Omega,\Omega_0) = R_m(\tau(\lambda),\Omega,\Omega_0) + \frac{\alpha_N(\lambda)T_m(\tau(\lambda),\Omega_0)}{1-\alpha_N(\lambda)R_{m,\mathrm{diff}}(\tau(\lambda))}T_{\mathrm{m,beam}}(\tau(\lambda),\Omega), \quad (2)$$

where $\tau(\lambda)$ is the molecular optical depth above clouds; $\alpha_N(\lambda)$ is the narrowband cloud albedo for wavelength λ of MODIS aerosol bands; $\mathbf{\Omega_0}$ and $\mathbf{\Omega}$ are the direction of the Sun and the viewing direction of the satellite; μ is cosine of the satellite viewing zenith angle; R_m is the reflectance of the molecular layer; T_m and $T_{m,\mathrm{diff}}$ are transmittances of the molecular layer for collimated sunlight from above and diffuse radiation reflected from the cloud layer below, respectively; $R_{m,\mathrm{diff}}$ is the reflectance of the molecular layer for diffuse radiation from below; and $T_{m,\mathrm{beam}}$ is the beam transmittance (or extinction), as defined by *Thomas and Stamnes* [1999], of the molecular layer for reflected radiation from the cloud layer below to the direction of satellite, and $T_{m,\mathrm{beam}}(\tau(\lambda),\mathbf{\Omega}) = e^{-\frac{\tau(\lambda)}{\mu}}$.

[8] R_1 is the same as in *Marshak et al*. [2008, equation (3)]. The denominator in the second term of equation (1) accounts for multiple reflections between the broken cloud field and the molecular layer in computing reflectance due to scattering and extinction. This multiple reflection effect was neglected in computing the radiance that causes only extinction (no scattering) in the earlier study and now is included by adding the same denominator in equation (2).

[9] Here we use $T_{m,\mathrm{diff}}$ and $T_{m,\mathrm{beam}}$ to distinguish diffuse transmittance and beam transmittance; the later includes only extinction without scattering. Thus, the enhancement (ρ or ΔR) can be expressed as follows:

$$\rho = \Delta\mathrm{R}(\lambda,\Omega,\Omega_0) = R_1 - R_2 = \frac{\alpha_N(\lambda)T_m(\tau(\lambda),\Omega_0)}{1-\alpha_N(\lambda)R_{m,\mathrm{diff}}(\tau(\lambda))}\left[T_{m,\mathrm{diff}}(\tau(\lambda),\Omega) - T_{m,\mathrm{beam}}(\tau(\lambda),\Omega)\right], \quad (3)$$

where the expressions of transmittances and reflectance are summarized in Table 1 for clarity.

[10] It is evident that the cloud-induced clear-sky reflectance enhancement is a function of wavelength primarily through the strong wavelength dependence of molecular scattering optical depth. Since the molecular scattering optical depth is inversely proportional to the fourth power of the wavelength, this type of 3-D cloud radiative effect is negligible for 0.87 μm and longer wavelengths. Thus, we perform a correction only for clear-sky reflectance for MODIS bands at 0.47, 0.55, 0.66 μm. Since cloud albedo depends weakly on wavelength in visible bands, we ignore the wavelength dependence in cloud albedo and refer to cloud albedo in MODIS visible bands as narrowband albedo.

Table 1. Expression of Transmittances and Reflectance for Molecular Layer With Optical Depth of $\tau_0 = \tau(\lambda)$[a]

	Name	Input Flux (Source)	Expression
$T_m(\tau_0, \mathbf{\Omega_0})$	Flux transmittance	$\boldsymbol{F_0}$ (Beam flux)	$F(\tau=\tau_0)/F_0\cos(\Omega_0)$
$T_{m,\mathrm{diff}}(\tau_0, \mathbf{\Omega})$	Radiance transmittance	$\boldsymbol{F_0}$ (Isotropic flux)	$\pi I(\tau=\tau_0,\Omega)/F_0$
$R_{m,\mathrm{diff}}(\tau_0)$	Reflectance	$\boldsymbol{F_0}$ (Isotropic flux)	$F(\tau=0)/F_0$
$T_{m,\mathrm{beam}}(\tau_0, \mathbf{\Omega})$	Beam transmittance	$\boldsymbol{I_0}$ (Beam radiance)	$\exp(-\tau_0/\cos(\Omega))$

[a]Note that T_m and $T_{m,\mathrm{diff}}$ include scattered radiation, and the beam transmission $T_{m,\mathrm{beam}}$ is purely due to extinction. $\mathbf{\Omega_0}$ and $\mathbf{\Omega}$ are the direction of the Sun and the viewing direction of the satellite.

[11] Computation of reflectance and transmittances for the molecular layer in equation (3) is straightforward. However, the estimation of narrowband cloud albedo in a broken cloud field is rather challenging due to the highly inhomogeneous nature of broken cloud fields. Here we take advantage of shortwave flux observations from the Clouds and the Earth's Radiant Energy System (CERES) instrument flying on the same satellite. The following describes how we estimate narrowband flux or albedo in broken cloud fields.

2.2. Broadband-to-Narrowband Flux Conversion

[12] CERES provides instantaneous top-of-atmosphere (TOA) radiative fluxes [*Wielicki et al*., 1996; *Loeb et al*., 2005; *Minnis et al*., 2011]. However, the CERES broadband TOA shortwave flux is not readily applicable for computing the clear-sky reflectance enhancement in equation (3), where the narrowband flux is required. It is necessary to convert CERES broadband flux to narrowband flux. While this conversion and the coarser-resolution CERES data cause some uncertainties in our method (see section 5), using CERES data allows us to benefit from the statistically robust, unbiased angular models of reflected radiance that CERES uses for converting broadband radiances into fluxes.

[13] The broadband shortwave radiation field is not independent from spectral radiation fields. The broadband shortwave radiance and flux are the integrals of their spectral components over solar spectral wavelengths. Earlier studies also found that broadband radiance and flux are functions of narrowband values, and regression methods were applied in performing narrowband-to-broadband conversions to derive TOA shortwave albedos from narrowband radiance observations [e.g., *Minnis and Harrison*, 1984; *Li and Leighton*, 1992; *Loeb et al*., 2006; *Sun et al*., 2006].

[14] The narrowband-to-broadband conversion studies also suggest that it is possible to make broadband-to-narrowband conversion. In the correction algorithm, we convert broadband flux to narrowband flux, assuming that the flux ratio for broken cloud field (i.e., narrowband flux F_N to broadband flux F_B) is equal to a modeled plane-parallel flux ratio (i.e., modeled narrowband flux F_N^m to modeled broadband flux F_B^m) as expressed in equations (4a) and (4b). Note that a similar assumption was used to compute the clear-sky reflectance enhancement in broken cloud fields by *Kassianov and Ovtchinnikov* [2008]. They found that the ratio between the two 1-D reflectances at two wavelengths was a good approximation to the 3-D ratio of the same wavelengths, although the two reflectances were quite different.

$$\frac{F_N}{F_B} = \frac{F_N^m}{F_B^m} \tag{4a}$$

or

$$F_N = \frac{F_N^m}{F_B^m} F_B. \tag{4b}$$

Equation (4b) for fluxes can also be expressed in albedos in equation (4c)

$$\alpha_N = \frac{\alpha_N^m}{\alpha_B^m} \alpha_{\mathrm{CERES}}, \tag{4c}$$

where α_N^m and α_B^m are plane-parallel albedos, α_{CERES} stands explicitly for CERES broadband albedo, and α_N is the estimated narrowband albedo.

[15] For a given solar zenith angle of θ_0, cloud fraction of f, and cloud optical depth of τ_c, the modeled TOA narrowband and broadband fluxes in a broken cloud field are computed as a linear combination of clear sky and cloudy atmosphere fluxes as

$$F_N(\theta_0, \tau_c, f) = (1-f)F_n(\theta_0, 0) + fF_n(\theta_0, \tau_c) \tag{5a}$$

$$F_B(\theta_0, \tau_c, f) = (1-f)F_b(\theta_0, 0) + fF_b(\theta_0, \tau_c), \tag{5b}$$

where $F_n(\theta_0, \tau_c)$ and $F_b(\theta_0, \tau_c)$ denote upward narrowband and broadband fluxes computed using the discrete ordinate radiative transfer model [*Stamnes et al*., 1988] for plane-parallel clouds.

[16] The plane-parallel model computes narrowband albedos for a set of visible cloud optical depth from 0 up to 158, similar to those in the current lookup table for the MODIS cloud retrieval algorithm. The cloud water droplets are assumed to have a lognormal distribution with effective variance of 0.11 and effective radius of 10 μm. We assume a water cloud layer at 1–2 km over the ocean and apply an ocean bidirectional reflectance distribution function model with a surface wind speed of 7 m/s. We use a correlated-k method to compute broadband albedos.

[17] CERES Single Satellite Footprint TOA/Surface Fluxes and Clouds (SSF) data provide instantaneous TOA shortwave flux (F_B), as well as cloud optical depth and cloud fraction retrieved from MODIS observations are aggregated in the CERES field of view (FOV) [*Geier et al*., 2003; *Minnis et al*., 2011]. To reduce errors due to cloud inhomogeneity, we use the logarithmic averaged cloud optical depth in CERES SSF data to compute narrowband and broadband fluxes (F_N^m and F_B^m) [*Cahalan et al*., 1994]. The narrowband flux (F_N) at CERES FOV is computed using equation (4b).

[18] At present, we assume that the upward narrowband flux is uniformly distributed within the CERES 20 km footprint. Accordingly, we assign to each 1 km × 1 km MODIS pixel the narrowband flux of the CERES footprint with the closest center. The narrowband flux for each MODIS 10 km × 10 km box is then obtained as the average of 1 km pixel values within the box.

2.3. Correction of MODIS Spectral Reflectance and Aerosol Retrieval

[19] Before proceeding to correcting the 3-D effects on aerosol property retrievals, we briefly review the MODIS aerosol over ocean algorithm. The MODIS aerosol over ocean algorithm uses clear-sky reflectance at six wavelengths to retrieve aerosol properties for 10 km × 10 km boxes. In the operational process, a series of tests is performed to exclude cloudy, sediment, and sun glint pixels. The reflectance at each wavelength is averaged over pixels that have passed all tests in a 10 km × 10 km MODIS box. Given six-band reflectances, the MODIS aerosol algorithm searches for the best solution of one fine mode and one coarse mode, weighted by optical depth, from 20 combinations of four fine-mode models and five coarse-mode models [*Remer et al*., 2005].

[20] With the narrowband flux obtained from equation (4b), we compute the cloud-induced clear-sky enhancement from equation (3). Subtracting the enhancement, $\Delta R(\lambda)$, from

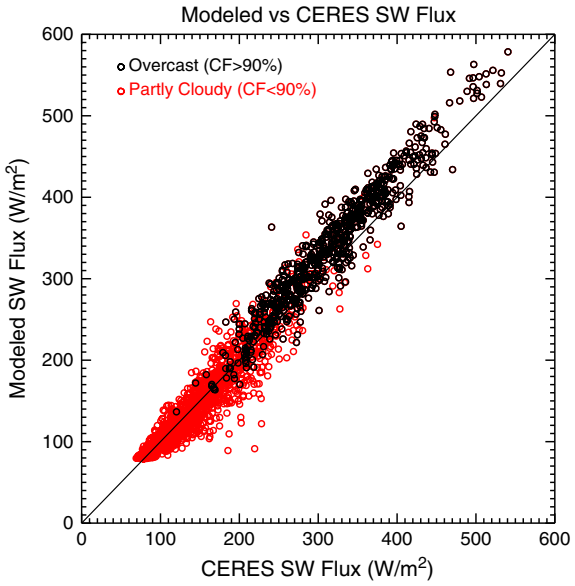

Figure 2. Modeled broadband flux versus CERES observations colocated with the MODIS image acquired on 23 July 2007 1425 UTC off the coasts of Namibia in Figure 4. The red and black circles are for partly cloudy and overcast areas, respectively.

the MODIS-observed reflectance, $R_{\mathrm{MODIS}}(\lambda)$, we obtain a set of corrected reflectances:

$$R(\lambda) = R_{\mathrm{MODIS}}(\lambda) - \Delta R(\lambda). \tag{6}$$

[21] A set of corrected reflectances, along with solar and satellite viewing geometry, is used as inputs to the existing MODIS aerosol algorithm to retrieve aerosol optical properties. Here we briefly summarize the steps in the algorithm.

[22] First, we decide whether we need to make a correction for each MODIS 10 km × 10 km box. The requirements to make a correction for aerosol retrieval for a MODIS 10 km × 10 km box are as follows: (1) MODIS has an operational aerosol retrieval, (2) the box is partly cloudy (equivalently partly clear) as identified from MODIS cloud product, (3) the cloud top is below 3 km, and (4) aerosols are embedded in the boundary layer below the cloud top (based on CALIPSO observations). The algorithm checks all MODIS 10 km × 10 km boxes, and the correction is made to a box if it meets all four criteria; otherwise, no correction is made to that box. In the second step, we convert the CERES shortwave flux (or albedo) to narrowband flux (or albedo) in the CERES footprint as described in section 2.2. Third, we compute the cloud-induced clear-sky reflectance enhancements from equation (3). We then subtract the enhancements from the average spectral reflectance in MODIS 10 km × 10 km to obtain a set of corrected average spectral reflectances. Finally, we use the corrected reflectances as input to the MODIS aerosol retrieval algorithm to obtain the corrected aerosol properties.

[23] The current correction algorithm applies only to cloud-induced clear-sky enhancement due to the interaction between clouds and the molecular layer above. At present, it does not account for the enhancement due to interactions between clouds and the ocean surface and/or between clouds and aerosols. Since molecular Rayleigh scattering optical depth is inversely proportional to the fourth power of the wavelength, and the wavelength dependence of the ocean surface reflectance is much weaker than reflectance by Rayleigh molecules, our algorithm does not provide correction for all spectral reflectances. In particular, the longer wavelengths (near-IR) remain uncorrected in the present version of our method, and the spectral shape of reflectance is skewed towards shorter wavelengths. This can lead to unrealistic spectral properties in the retrieved aerosol optical depth (AOD). To make the aerosol retrieval process more robust, we keep the fine and coarse modes obtained by MODIS operational retrieval and allow the retrieval algorithm to adjust only the small mode aerosol fraction (SMAF) of AOD at 0.55 μm. The application of the algorithm is described in section 4.

3. Model Versus Observation for Consistency Check

[24] Before proceeding to apply the two-layer model to correct for the clear-sky radiance enhancement in aerosol retrievals, we perform a consistency check to compare modeled radiative fluxes and radiances with observations. Such a check is necessary to ensure that the model produces reasonable results and the assumptions are reasonable.

[25] Figure 2 presents modeled and CERES-observed shortwave fluxes for the MODIS granule described in section 4. It is evident that modeled and observed shortwave fluxes are highly correlated. Both modeled and observed shortwave fluxes range from ~80 W/m^2 to ~600 W/m^2. The scattered points with small shortwave flux represent clear sky. As the cloud amount increases in the CERES FOV, the reflected shortwave flux increases. The scattered points with a large shortwave flux represent overcast pixels with large cloud optical depth. Generally, the modeled shortwave flux is consistent with the observations except for large values of flux for which modeled values are biased higher than observations. Since we use a 1-D model to compute the flux, the discrepancies between the model and observation are likely due to cloud inhomogeneity or 3-D effects, although other model assumptions may also play a role. Though we do not have narrowband flux observations, we expect that the modeled and observed narrowband fluxes have a similar close relationship. This also implies that in broken cloud fields, the narrowband flux will be estimated more accurately by the equal ratio method in equation (4a) than by plane-parallel computations.

[26] The equal ratio of equation (4a) is a key assumption in converting broadband flux to narrowband flux. One may expect that the equal ratio assumption also applies to radiances, as demonstrated by *Kassianov and Ovtchinnikov* [2008]. Thus, the equal ratio for radiance is a necessary condition for equation (4a) to be valid. Simultaneous CERES broadband radiance and MODIS narrowband radiance weighted by the CERES point spread function are available in the SSF data set, which provides a good opportunity to perform the consistency check for the equal ratio assumption for radiances.

[27] We examine the relationships between narrowband radiance and broadband radiance for both observed and modeled results in Figure 3. It is clear that observed narrowband and broadband radiances are well correlated similarly to the results in *Loeb et al.* [2006, Figure 1b]. It is also evident that modeled narrowband and broadband radiances are also well correlated, as the points of modeled and observed

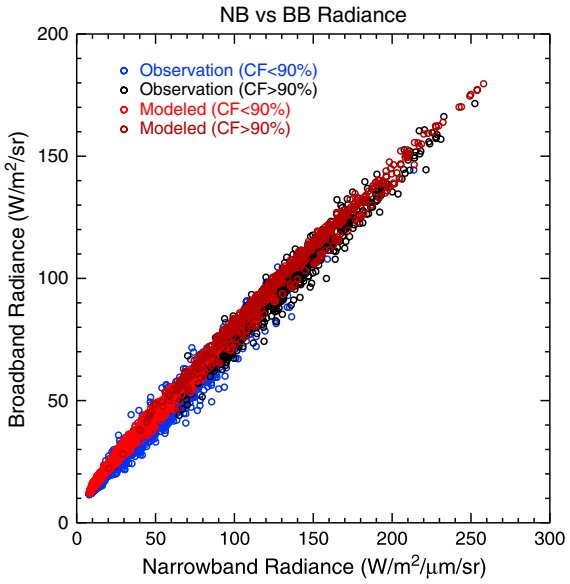

Figure 3. Modeled (blue) and CERES- and MODIS-observed (red) broadband and narrowband radiances for colocated CERES and MODIS observations acquired on 23 July 2007 1425 UTC off the coasts of Namibia in Figure 4. The observed radiances are blue and black circles for partly cloudy and overcast areas, respectively. The modeled radiances are red and brown circles for partly cloudy and overcast areas, respectively.

radiances are scattered around the diagonal line. The observed broadband-to-narrowband radiance ratio of 0.67, which is the slope of the best fit, is close to the ratio of 0.69 computed from 1-D radiative transfer models. This suggests that even though the 1-D model may not produce accurate TOA radiances, the modeled broadband-to-narrowband radiance ratio is close to the observations. Therefore, the results are consistent with the equal ratio assumption in equation (4a).

4. Application to MODIS Images

[28] Since boundary layer clouds are common off the west coasts of continents, those regions are ideal for testing the correction algorithm. We use MODIS images and simultaneous CERES observations to demonstrate the process of correcting MODIS aerosol retrievals for 3-D cloud effects. Here we use a granule of Aqua MODIS (23 July 2007 1425 UTC) off the coasts of Namibia to demonstrate the algorithm. A true color image of the granule is shown in Figure 4. It is evident that the eastern one third of the image is covered with extensive stratocumulus clouds. Farther away from the coasts of Namibia, there are more clear areas, except for a large strip of stratocumulus that stretches from the center to the northwest corner of the image.

[29] CALIPSO observations are used to confirm that clouds are in the boundary layer and aerosols are trapped below cloud top at about 2 km in the overlap region of CALIPSO and MODIS (Figure 4, right panel). The cloud top height identified by CALIPSO observations is used for estimating molecular optical depth above clouds in equation (3). It is important to note that, although cloud height can be estimated from the MODIS cloud product, only CALIPSO observation can provide reliable aerosol height near clouds. Thus, CALIPSO observations are very helpful for correcting 3-D cloud radiative effects.

[30] MODIS-retrieved cloud optical depth and aerosol optical depth are presented in Figure 5. The cloud cover of this granule is about 46%. The average cloud optical depth is 8.1 with a standard deviation of 7.7. The average aerosol optical depth at 0.55 μm is 0.11 with a standard deviation of 0.08. It is interesting to note that MODIS aerosol optical depth in the upper right quadrant is much higher than in the rest of the granule.

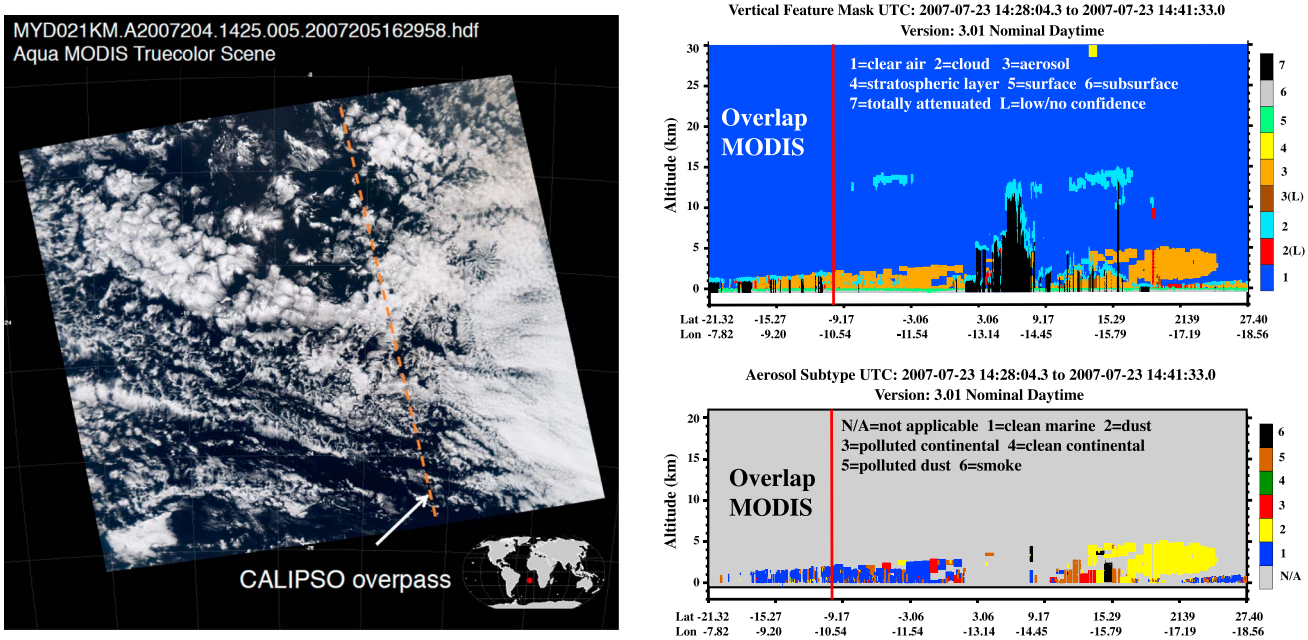

Figure 4. (left) MODIS granule acquired from Aqua MODIS on 23 July 2007 1425 UTC with CALIPSO overpass indicated. (right) CALIPSO observations show that clouds and aerosols are trapped in the boundary layer below 2 km. Regions overlapped with MODIS are indicated.

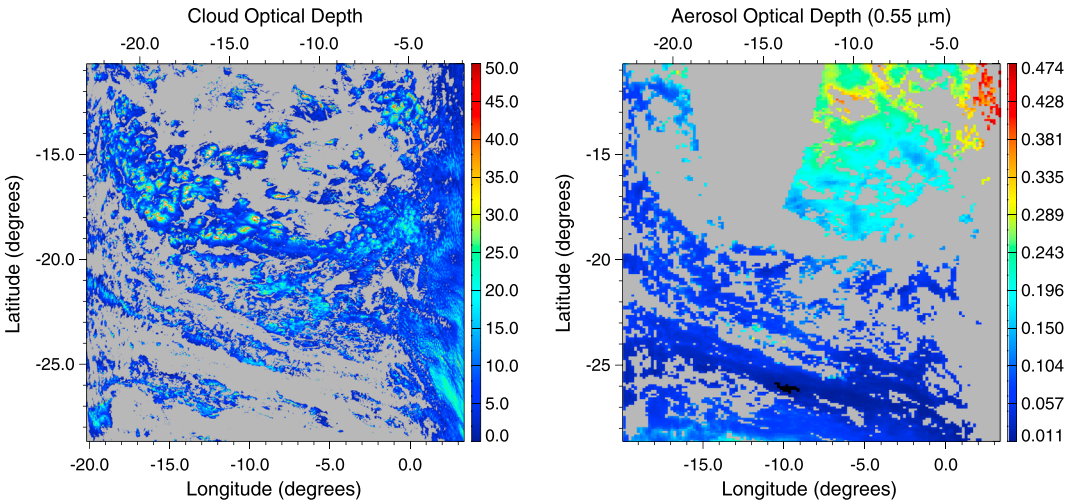

Figure 5. (left) MODIS cloud optical depth field. The cloud cover is ~46%. The average cloud optical depth is 8.1 with a standard deviation of 7.7. (right) Aerosol optical depth field retrieved by the operational algorithm. The average aerosol optical depth at 0.5 μm is 0.11 with a standard deviation of 0.08.

4.1. Broadband-to-Narrowband Conversion

[31] The narrowband albedo is obtained from CERES broadband flux using the ratio relationship of equation (4a). The scatterplot of narrowband and broadband albedos is presented in Figure 6. It shows that the narrowband and broadband albedos are highly correlated, which is consistent with the results in a narrowband-to-broadband conversion study [see *Sun et al*., 2006, Figure 1a].

[32] The image of the narrowband albedo used for correction is presented in the right panel of Figure 6. The histogram equalization technique is used for image enhancement, so that each increment in the color bar contains the same number samples. The narrowband albedo ranges from 0.07 up to 0.48. The average narrowband albedo is 0.16 with a standard deviation of 0.05.

4.2. Compute Reflectance Enhancement

[33] Once the narrowband albedo is obtained, we compute the cloud-induced clear-sky reflectance enhancement using equation (3). The average 0.55 μm reflectance used for MODIS operational aerosol retrievals in 10 km × 10 km boxes and the associated reflectance correction are presented in Figure 7. Boxes without retrieval are indicated by gray color (Figure 7, left). The MODIS reflectance ranges from ~0.05 to ~ 0.17. Note that the gray triangle area in the upper left half of the image without aerosol retrieval is due to sun glint. The right panel of Figure 7 shows the corrections to the reflectance presented in the left panel. No correction is made to reflectances in a completely clear box as indicated in black in the right panel of Figure 7. It is interesting to note that the reflectance correction is positive for all boxes. The

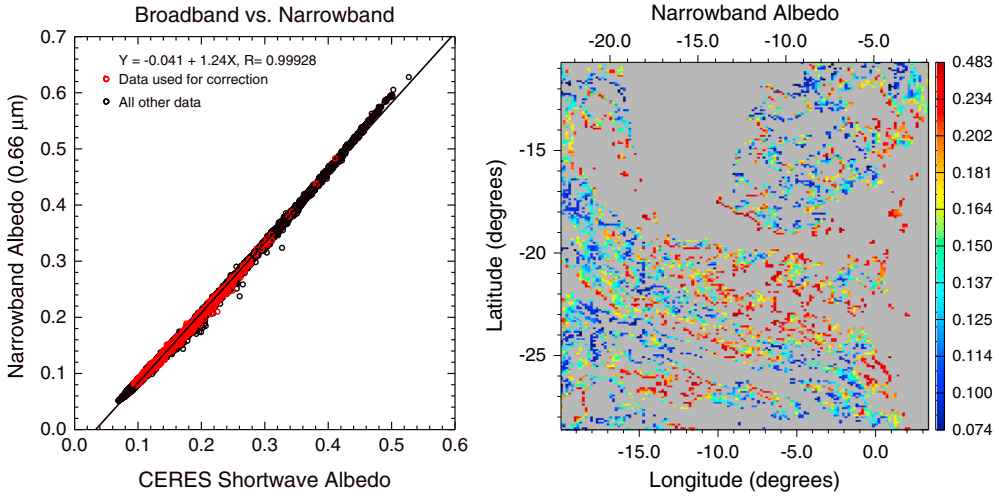

Figure 6. (left) Red circles are derived narrowband albedo versus CERES shortwave albedo for the MODIS 10 km boxes where correction is applied, and black circles are for all other data in the MODIS granule. (right) Image of narrowband albedo applied to the reflectance correction. The average of narrowband albedo is 0.16 with a standard deviation of 0.05.

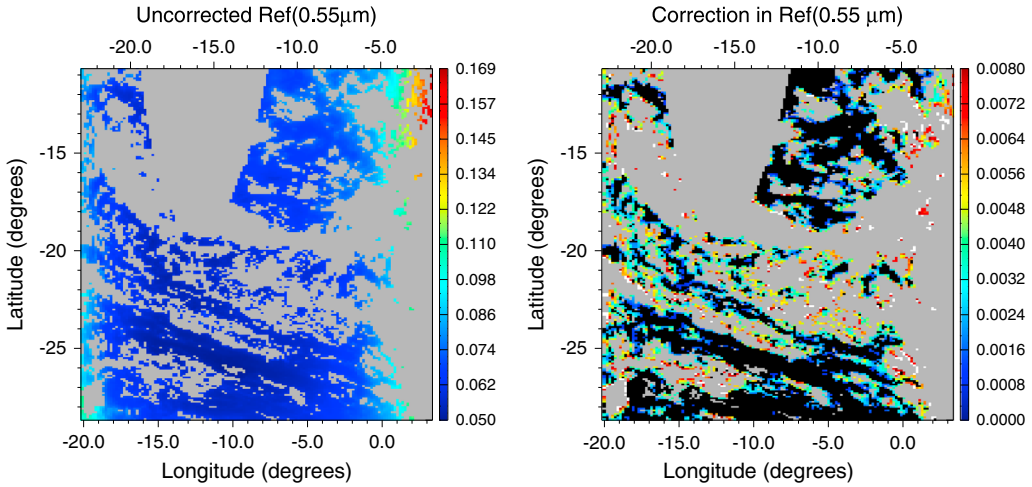

Figure 7. (left) Uncorrected MODIS reflectance at 0.55 μm. (right) The correction of reflectance. The average reflectance correction is 0.004 with a standard deviation of 0.002. Pixels (~2.4%) with reflectance correction values above the upper bound of the color bar (0.008) up to 0.016 are indicated in white.

correction ranges from 0 to 0.016 with an average of 0.004 and a standard deviation of 0.002 (Figure 7, right).

[34] The scatterplots of the MODIS apparent reflectance and corrected reflectance are presented in Figure 8 for 0.55 and 0.66 μm. The color scheme used is such that dark blue represents small correction and brown represents large correction. It is clear that the corrected reflectance is always less than the original observed apparent reflectance. The correction for the shorter wavelength is larger than that for the longer wavelength.

4.3. Retrieval of 3-D Corrected Aerosol Optical Properties

[35] Using a set of corrected reflectances together with solar and viewing angles as input to the offline version of the operational MODIS aerosol retrieval code [*Remer et al.*, 2005], we obtained the corrected aerosol properties including AOD, the Ångström exponent, and the SMAF. We compare the original AOD from the operational algorithm with the corrected AOD at wavelengths 0.55 and 0.66 μm in Figure 9.

[36] While one may expect that the correction would always lead to a smaller spectral AOD since the reflectance correction is always positive for all wavelengths, we found that this is not necessarily true. Indeed, on average the correction leads to a smaller AOD for all wavelengths, but it can also lead to an increase of AOD as shown in Figure 9. This is not surprising. The MODIS aerosol retrieval algorithm over the ocean uses reflectances from six bands. For a given set of reflectances, the retrieval algorithm selects the best pair of fine and coarse models (weighted by optical depth) from 20 combinations of four fine-mode and five coarse-mode models. In order to be consistent with the operational retrieval, we chose the same best pair of fine and coarse aerosol models as those in the operational retrieval, allowing the MODIS algorithm to find the best partitioning of the fine mode and coarse AOD based on corrected reflectances. For the same aerosol models, the MODIS algorithm finds a different partition of the AOD for a set of corrected reflectances as shown in section 4.4. Thus, the overall aerosol size distribution for a set of corrected reflectances is different from that for a set of uncorrected reflectances. This could eventually lead to larger AODs due to the difference in scattering phase functions, which are attributed to the difference in aerosol size distributions between the operational retrieved aerosol and the corrected one.

[37] The images of the corrected AOD and the correction of AOD (operational minus corrected) at 0.55 μm are presented in Figure 10. Note that no correction is made to MODIS-retrieved AOD in clear 10 km × 10 km boxes indicated in black. It is not trivial to visualize the difference between operationally retrieved (Figure 5, right) and corrected (Figure 10, left) AODs. Here we focus on the image of AOD correction in the right panel of Figure 10. The correction of AOD ranges from −0.035 up to 0.094 with an average value of 0.003 and a standard deviation of 0.013. Comparing this with the original MODIS-retrieved AOD in Figure 5, we find that the larger values of correction are in the upper right quadrant of the image, where aerosol loading is also larger. However, this does not necessarily mean that AOD correction is positively correlated with AOD. Unlike the reflectance correction that is strongly correlated to cloud albedo, the correction of AOD depends not only on nearby cloud properties, but also on aerosol properties. This is because the MODIS aerosol algorithm uses multispectral reflectance to retrieve aerosol properties [*Remer et al.*, 2005]. Even for the same reflectance correction in visible wavelengths, the MODIS aerosol algorithm will find a different AOD correction if the corrected spectral reflectances are not the same. Since aerosol type determines spectral reflectance shape (e.g., the reflectance of fine-mode aerosol has much stronger wavelength dependence than the reflectance of coarse-mode aerosol), AOD correction will depend on aerosol properties as well. In fact, aerosols in the upper right quadrant, where large AOD correction is found, are different from aerosols in the rest of the image as one can see from the Ångström exponent and SMAF shown in Figures 11 and 13. Note that the two-layer model only corrects spectral radiances. The spectral AOD correction depends very much on the specifics of the MODIS aerosol retrieval algorithm. We are working on a research mode of the aerosol retrieval algorithm that will be more sensitive to the correction of spectral radiances.

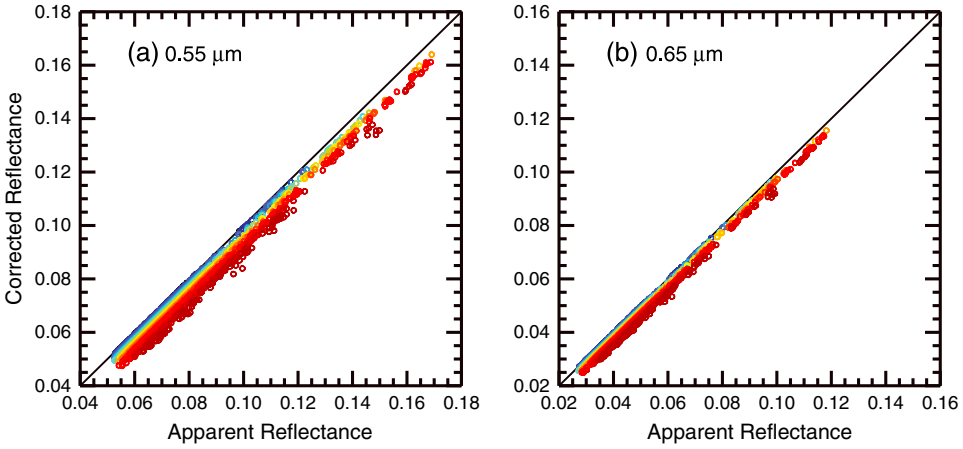

Figure 8. (left) Corrected reflectance versus MODIS-observed apparent reflectance at 0.55 μm. (right) Similar to the left panel but for 0.65 μm. The color scheme is such that blue represents small correction and brown represents large correction.

4.4. Ångström Exponent and Small Mode Aerosol Fraction

[38] Here we examine the Ångström exponent and SMAF. The MODIS product provides the Ångström exponent for two pairs of wavelengths, i.e., 0.55 versus 0.87 μm and 0.87 versus 2.13 μm. Since we do not make a correction to the radiance for 0.87 μm and longer wavelengths, we examine the Ångström exponent for 0.55 μm/0.87 μm.

[39] The image of the Ångström exponent from MODIS operational retrieval is presented in the left panel of Figure 11, with values greater than 1 indicated by white. The value of the Ångström exponent ranges from −0.13 to 2.8 with an average of 0.64 and standard deviation of 0.32. We find that larger values of the Ångström exponent are mostly in the upper right quadrant of the image.

[40] The image of the correction of the Ångström exponent (operational minus corrected) is presented in the right panel of Figure 11. The average correction is 0.33 with a standard deviation of 0.25. We find that most of the large values of correction are in the lower half of the image. Although there are some large correction values in the upper right quadrant of the image from the MODIS operational retrieval, the average correction of the Ångström exponent in this area is small.

[41] We examine the three frequency distributions of the Ångström exponent in Figure 12. The green line is the distribution for all completely clear 10 km × 10 km MODIS boxes for which no correction is involved. The other two are for operational retrieval and corrected aerosols for a partly cloudy atmosphere. For partly cloudy atmosphere, the distribution of the Ångström exponent from MODIS operational retrievals is indicated by the red line, and the corresponding corrected distribution is the blue line.

[42] First, we examine the pair of distributions from MODIS operational retrievals (red and green in Figure 12). For partly cloudy atmosphere, the Ångström exponent has an average value of 0.64 with a standard deviation of 0.32. For completely clear atmosphere, the Ångström exponent has an average value of 0.61 with a standard deviation of 0.38. The modal and average values of the Ångström exponent for partly cloudy box are larger than those for completely clear box. Since the Ångström exponent is inversely related to the average size of aerosol particles,

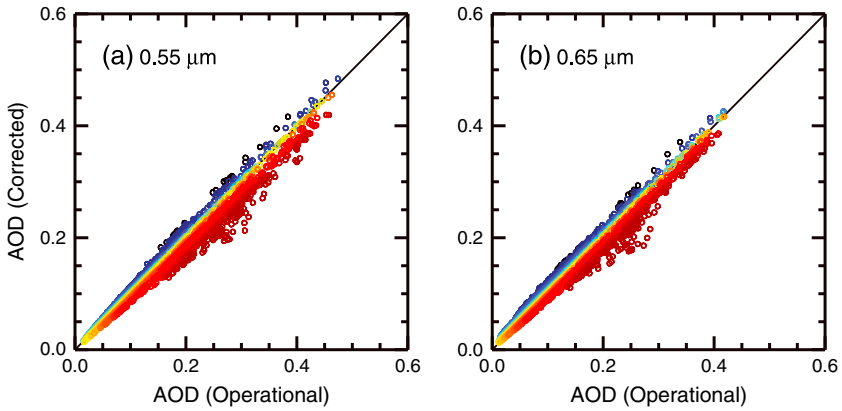

Figure 9. (left) Comparison of the operational MODIS AOD and the corrected AOD at 0.55 μm. (right) Similar to the left panel but for 0.66 μm. A color scheme is used such that blue represents small correction (negative for AOD correction) and red represents large correction.

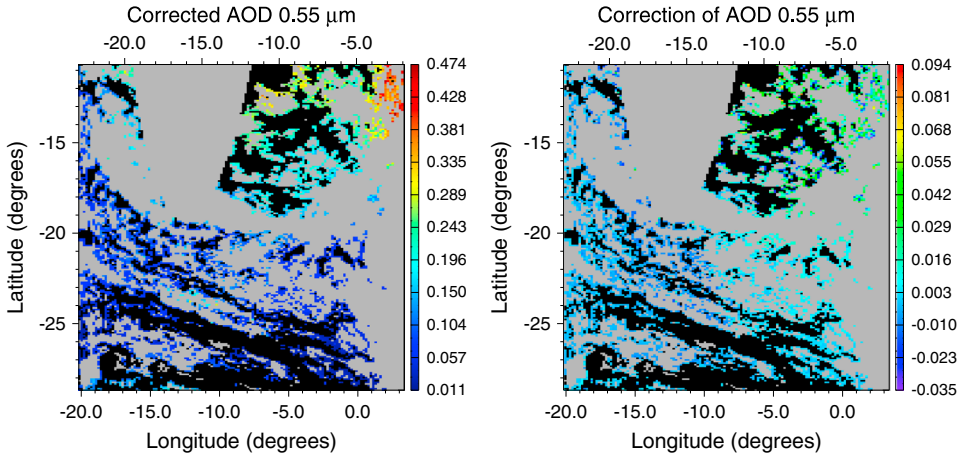

Figure 10. (left) Corrected AOD at 0.55 μm. (right) Correction of AOD (operational minus corrected) at 0.55 μm with the average of 0.003 and a standard deviation of 0.013. Clear areas are indicated in black.

theoperational retrievals suggest a smaller apparent aerosol particle size in partly cloudy MODIS 10 km × 10 km boxes as compared to completely clear regions. This is the so-called "bluing effect" described by *Marshak et al*. [2008].

[43] When we examine the distribution of the corrected Ångström exponent for partly cloudy atmosphere, we find that the distribution shifts to lower values (average of 0.32) with a narrower spread (standard deviation of 0.27) as compared to the original distribution (average of 0.64 and standard deviation of 0.32) for the same partly cloudy atmosphere. It is important to note that the average corrected Ångström exponent for partly cloudy atmosphere is smaller than the average Ångström exponent for completely clear atmosphere, which suggests larger aerosol particles near clouds after the correction. The increase of aerosol particles indicated by the Ångström exponent is consistent with the decrease of the SMAF presented in Figure 14.

[44] Images of SMAF are presented in Figure 13. The original MODIS operational retrieved SMAF has an average value of 0.44 with a standard deviation of 0.13 (Figure 13, left). We find larger values of the SMAF in the upper left quadrant, which is similar to the pattern for the Ångström exponent. This similarity is due to the fact that the Ångström exponent is inversely related to the average size of aerosol particles as mentioned earlier.

[45] The image of the correction of SMAF is presented in the right panel of Figure 13. The average of SMAF correction is 0.17 with standard deviation of 0.11. We find that most of the large values of the correction are in the lower half of the image, yielding small values of the SMAF in this area after the correction.

[46] We examine three frequency distributions of SMAF in Figure 14, one for operational retrieval in completely clear

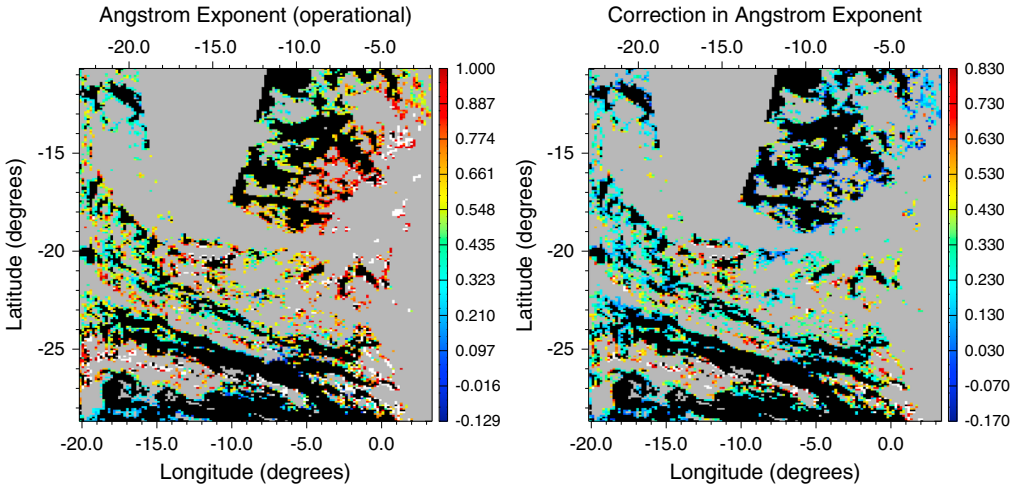

Figure 11. (left) MODIS operational retrieved Ångström exponent for 0.55 μm/0.87 μm (mean = 0.64, standard deviation = 0.32). (right) Correction of Ångström exponent (operational minus corrected) (mean = 0.32, standard deviation = 0.25). A small fraction of data exceeding the upper value of the color bar is indicated in white.

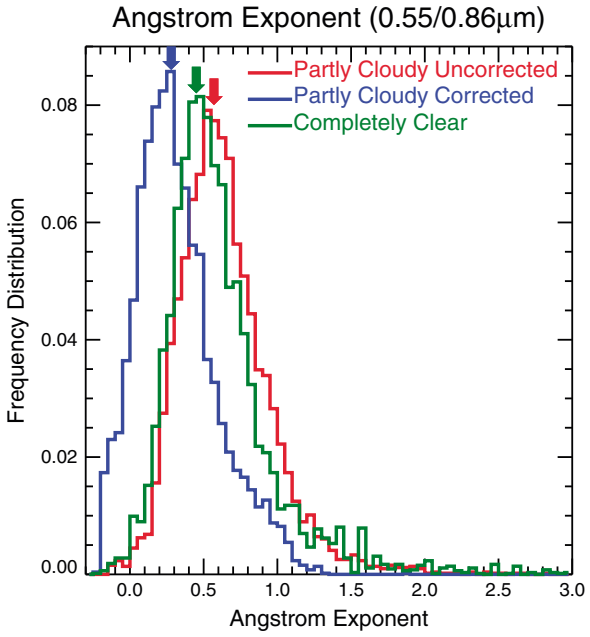

Figure 12. Frequency distributions of Ångström exponent for 0.55 μm/0.87 μm. For partly cloudy atmosphere, the distribution of MODIS retrieved Ångström exponent (mean = 0.64, standard deviation = 0.32) is shown in red, that of the corrected Ångström exponent (mean = 0.32, standard deviation = 0.27) is in blue. For completely clear atmosphere, the distribution of MODIS retrieved Ångström exponent (mean = 0.61, standard deviation = 0.38) is in green.

atmosphere with no correction involved and the other two for operational retrieval and corrected values for partly cloudy atmosphere. For completely clear atmosphere, the frequency distribution is plotted in green. For a partly cloudy atmosphere, the distribution of SMAF from MODIS operational retrieval is plotted in red, and the distribution for corrected SMAF is in blue.

[47] First, we examine the distributions of SMAF from the MODIS operational retrieval. The distributions for both partly cloudy and completely clear areas are similar, but some differences do exist. Above the value of ~0.3, the frequency distribution for partly cloudy atmosphere (red) is almost always larger than that for a completely clear atmosphere (green), except for two bins near the distribution mode and two bins near 0.5 and 0.65. The average value of SMAF for partly cloudy atmosphere is 0.44, 0.01 larger than the average value of 0.43 for completely clear atmosphere. Thus, the MODIS operational retrieved average values of the Ångström exponent, SMAF, and AOD (not shown here) are larger in partly cloudy MODIS 10 km × 10 km boxes than in completely clear areas, consistent with an earlier study by *Loeb and Schuster* [2008].

[48] Next we examine the distribution of corrected SMAF for partly cloudy areas. The distribution shifts to lower values, with an average of 0.27, as compared to the average value of 0.44 for the original distribution and an average value of 0.43 for completely clear atmosphere. The decrease in SMAF after the correction is equivalent to an increase in coarse-mode fraction of aerosol particles and is consistent with the decrease in the Ångström exponent presented earlier.

5. Uncertainty Analysis

[49] In this study, we use CERES broadband fluxes to estimate the narrowband flux values needed for computing the reflectance enhancements. However, CERES does not measure flux values directly, and angular distribution models (ADMs) are needed to convert CERES measured radiance values to fluxes. While these ADMs can have large instantaneous uncertainties, they are unbiased [*Loeb et al.*, 2007], which could help make narrowband fluxes and reflectance corrections unbiased as well. Although it is advantageous to use unbiased CERES fluxes, uncertainty in the broadband flux will lead to errors in estimating narrowband flux, and consequently errors in reflectance correction and AOD correction.

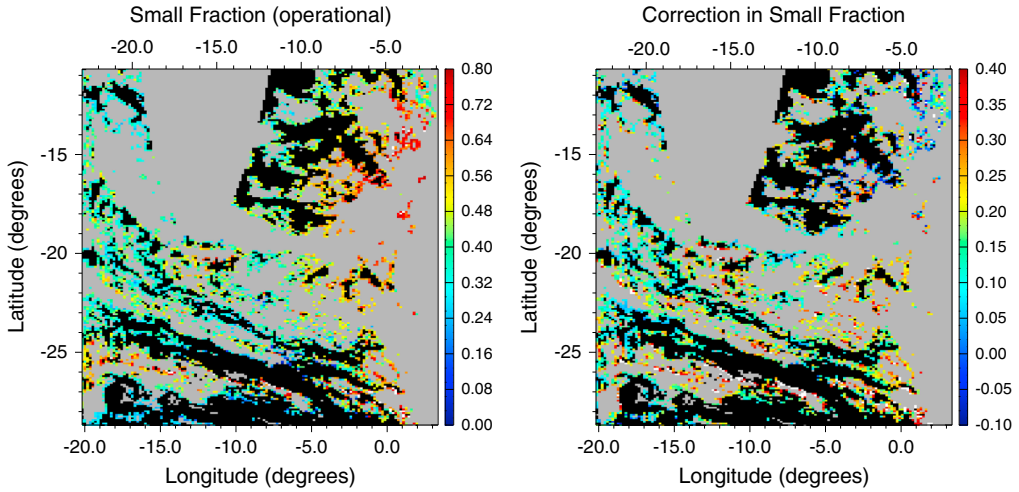

Figure 13. (left) MODIS operational retrieved SMAF of AOD at 0.55 μm (mean = 0.44, standard deviation = 0.13). (right) The correction of fraction of small mode AOD (operational minus corrected) (mean = 0.17, standard deviation = 0.11). A small fraction of data exceeding the upper value of the color bar is indicated in white.

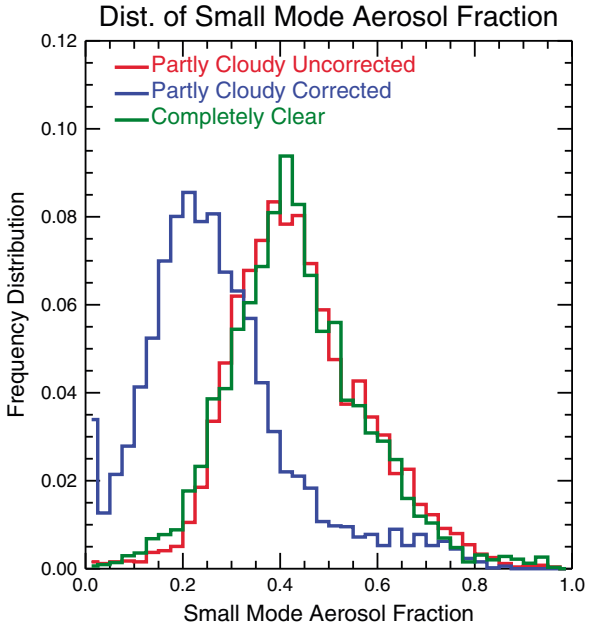

Figure 14. Frequency distributions of the SMAF of AOD at 0.55 μm. For partly cloudy atmosphere, the distribution of MODIS retrieved SMAF (mean = 0.44, standard deviation = 0.14) is shown in red, that of the corrected SMAF (mean = 0.27, standard deviation = 0.15) is in blue. For completely clear atmosphere, the distribution of MODIS retrieved SMAF (mean = 0.43, standard deviation = 0.14) is in green.

[50] Another source of uncertainty in reflectance correction and AOD correction is errors in the input parameters used in computing radiative fluxes.

[51] Here we estimate errors in reflectance correction and associated uncertainties in correction of aerosol properties. We consider two sources of uncertainty. One source of uncertainty is related to the errors in molecular scattering optical depth estimate above cloud top. Another source is related to the errors in narrowband albedo estimate. Taking the derivative of natural logarithm of both sides of equation (3), one can derive the relative uncertainty in reflectance correction as

$$\frac{\Delta\rho}{\rho}=\left[\frac{1}{T_m}\frac{\partial T_m}{\partial\tau_m}+\frac{\alpha_N}{1-\alpha_N R_{m,\mathrm{diff}}}\frac{\partial R_{m,\mathrm{diff}}}{\partial\tau_m}+\frac{1}{T_{m,\mathrm{diff}}-T_{m,\mathrm{beam}}}\left(\frac{\partial T_{m,\mathrm{dif}f}}{\partial\tau_m}-\frac{\partial T_{m,\mathrm{beam}}}{\partial\tau_m}\right)\right]\Delta\tau_m+\left(1+\frac{\alpha_N R_{m,\mathrm{diff}}}{1-\alpha_N R_{m,\mathrm{diff}}}\right)\frac{\Delta\alpha_N}{\alpha_N},\tag{7}$$

where $\Delta\tau_m$ is the uncertainty of estimated molecular optical depth above cloud due to the uncertainty of estimated cloud top pressure ΔP.

[52] The first term on the right-hand side of equation (7) is the uncertainty due to the error in estimation of molecular optical depth above cloud or error in cloud top pressure estimation. We found that the relative uncertainty in reflectance correction is proportional to the uncertainty in cloud top pressure estimate, and $\Delta\rho/\rho\approx 0.001\Delta P$, where ΔP is in hPa.

[53] The second term in equation (7) is the uncertainty due to the errors in narrowband albedo estimation. Using the equal ratio relation in equation (4c), one can show that

$$\frac{\Delta\alpha_N(\lambda)}{\alpha_N(\lambda)}\approx\left|\frac{\Delta\alpha_N^m(\lambda)}{\alpha_N^m(\lambda)}-\frac{\Delta\alpha_B^m(\lambda)}{\alpha_B^m(\lambda)}\right|+\left[\frac{\Delta\alpha_{\mathrm{CERES}}}{\alpha_{\mathrm{CERES}}}\right].\tag{8}$$

[54] The first two terms within the first absolute value symbol on the right-hand side of equation (8) are errors in the modeled narrowband and broadband albedo due to the uncertainty in input parameters such as cloud optical depth, aerosol optical depth, and column precipitable water vapor amount. Note that the signs in front of the relative uncertainty in modeled narrowband albedo and broadband albedo are different because of the ratio relation in equation (4c). Since both narrowband and broadband albedo are increasing functions of cloud optical depth [e.g., *Chakrapani et al*., 2002, Figure 4], errors in modeled narrowband and broadband albedo due to uncertainty in input cloud optical depth will cancel each other to some extent. A similar cancellation effect with smaller extent is expected for computing errors due to uncertainty in input aerosol optical depth and total column precipitable water vapor amount.

[55] The last term on the right-hand side of equation (8) is error due to uncertainty in CERES broadband flux using the ADMs. For broken low-level cloud fields, the uncertainty in CERES shortwave broadband flux is about 5% [see *Loeb et al*., 2006, Figure 4].

[56] We assume that uncertainties in input aerosol optical depth and water vapor only cause errors in clear-sky albedo computation since aerosols and water vapor are mostly in the boundary layer below cloud top. Thus, uncertainties in narrowband and broadband albedo can be expressed as summation of errors from different sources in equations (9a) and (9b), where the plane-parallel albedo is a function of cloud optical depth (τ_c), aerosol optical depth (τ_a), and total column precipitable water vapor amount (WV), and errors in cloudy and clear atmosphere albedo are weighted with cloud and clear fraction, respectively. Although cloud albedo depends strongly on solar zenith angle, we found that the relative uncertainty in reflectance correction does not have strong solar angle dependence. Uncertainty due to errors in total column precipitable water vapor amount does depend on solar angle. Still, we drop the solar zenith angle dependence of cloud albedo in equations (9a) and (9b) for simplicity:

$$\Delta\alpha_N^m=f\left|\frac{\partial\alpha_N^m(\tau_c,\tau_a,WV)}{\partial\tau_c}\Delta\tau_c\right|+(1-f)\left[\left|\frac{\partial\alpha_N^m(0,\tau_a,WV)}{\partial_{\mathrm{Ta}}}\Delta_{\mathrm{Ta}}\right|+\left|\frac{\partial\alpha_N^m(0,\tau_a,WV)}{\partial WV}\Delta\mathrm{WV}\right|\right],\tag{9a}$$

$$\Delta\alpha_B^m=f\left|\frac{\partial\alpha_B^m(\tau_c,\tau_a,WV)}{\partial\tau_c}\Delta\tau_c\right|+(1-f)\left[\left|\frac{\partial\alpha_B^m(0,\tau_a,WV)}{\partial_{\mathrm{Ta}}}\Delta_{\mathrm{Ta}}\right|+\left|\frac{\partial\alpha_B^m(0,\tau_a,WV)}{\partial WV}\Delta\mathrm{WV}\right|\right].\tag{9b}$$

[57] *Platnick et al*. [2004] show that uncertainty in MODIS water cloud optical depth is about 10%. There is a large

Table 2. Errors in Modeled Narrowband and Broadband Albedo Due to Different Sources of Uncertainty. Calculations Are for Low-Level Cloud With Cloud Top Height at 950 hPa and $\Delta P = 40$ hPa, Cloud Optical Depth of 10 and 10% Error in Cloud Optical Depth, and Aerosol Optical Depth of 0.1 At 0.55 μm, a Standard Atmosphere With Precipitable Water Vapor Amount of 0.5–4.5 cm, and the Cloud Fraction of 50%[a]

	$\Delta P = 40$ hPa	$\Delta\tau_c = 1$	$\Delta\tau_a = 0.1$	$\Delta WV = 4$ cm	$\Delta\alpha/\alpha$ (CERES)	Total
$\Delta\rho/\rho$	0.04	0.003	0.004	0.0265 (0.011)	0.055	0.13

[a]For errors due to uncertainty in precipitable water vapor amount, the value of 0.0265 is for a solar zenith angle of 60°, and the value of 0.011 in the parentheses is for a solar zenith angle of 30°. The larger value of 0.0265 is used to compute the total error of 0.13.

variability in precipitable water vapor amount. *King et al.* [2003] show that precipitable water vapor amount has large spatial and temporal variability, ranging from ~0.5 to ~4.5 cm in 80 MODIS cases from 1 April to 1 September 2002 over the southern Great Plains site of the Atmospheric Radiation Measurement Program. The error in aerosol optical depth retrieval over ocean is reported to be $\Delta\tau = \pm 0.03 \pm 0.05\tau$ [*Remer et al.*, 2005]. Errors in MODIS low-level boundary layer cloud top height are estimated to be 424 m for Collection 5 and 197 m for Collection 6 [*Baum et al.*, 2012]. We use some typical errors in input parameters to estimate relative error in reflectance correction. The results are summarized in Table 2. Overall uncertainty in reflectance correction is about 13%.

[58] Errors in reflectance correction will lead to relatively smaller errors in aerosol optical depth correction. This is because aerosol optical depth is approximately proportional to the reflectance (i.e., $\tau_a \propto R$). The relative error due to the uncertainty in reflectance correction can be expressed as

$$\frac{\Delta\tau_a}{\tau_a} = \frac{\Delta\rho}{R} = \frac{\rho}{R}\frac{\Delta\rho}{\rho}, \tag{10}$$

where R is the reflectance, ρ is the reflectance correction, and $\Delta\rho$ is the uncertainty in reflectance correction. Since the reflectance correction is typically about 10% (see Figure 7), the relative error purely due to errors in the reflectance correction is about 1%.

[59] We have also examined the error in the Ångström exponent due to uncertainties in the reflectance correction. We found that the error in the Ångström exponent is negligible compared to errors due to other sources of uncertainty reported in the literatures [e.g., *Ignatov and Stowe*, 2000; *O'Neill et al.*, 2001; *Schuster et al.*, 2006; *Wagner and Silva*, 2008]. This is largely due to the cancellation of positively correlated small errors (~1%) in spectral AOD correction while taking the ratio of AODs in computing the Ångström exponent.

6. Summary and Discussion

[60] We have implemented a two-layer algorithm for correcting aerosol properties for 3-D cloud radiative effects in the vicinity of clouds. This is the first time the algorithm has been applied to a full MODIS granule. We have highlighted the main steps of the algorithm, including the conversion of CERES broadband flux to visible narrowband flux, the estimation of clear-sky reflectance enhancement, and the correction of aerosol optical properties via an example of a granule off the coast of Namibia. We have performed a study to show that the assumption for broadband-to-narrowband flux conversion is consistent for modeled and observed radiances. This algorithm can be applied to both Terra and Aqua MODIS since simultaneous observations of shortwave flux from CERES are available from both satellites. For the Aqua satellite, we take advantage of CALIPSO observations for cloud and aerosol height information.

[61] The clear-sky reflectance correction is always positive and decreases with wavelength as a result of the wavelength dependence of molecular scattering optical depth. On average the correction leads to smaller AOD, Ångström exponent, and SMAF. It is worth noting that the correction may lead to larger spectral AOD. This is primarily due to a different scattering phase function resulting from different aerosol size distributions for the operational retrieved and corrected aerosols as described below.

[62] Since aerosols are usually optically thin, one may use the single scattering approximation for understanding this. In the single scattering approximation, for a nonreflective surface, the TOA reflectance is proportional to the product of phase function and aerosol optical depth [e.g., *Hansen and Travis*, 1974; *Kaufman et al.*, 1997]. One can show that the fine-mode aerosol scattering phase function is much larger than the coarse-mode aerosol phase function [e.g., *Sanghavi et al.*, 2013, Figure 2]. For a given reflectance, coarse aerosols with a smaller phase function will have a larger AOD compared to that for fine aerosols with a larger phase function. In a more general situation, aerosols consist of both fine and coarse modes. In this situation, for a given TOA reflectance, the aerosols with a smaller SMAF will have smaller phase function and larger AOD compared to aerosols with a larger SMAF.

[63] We also compared aerosol properties near clouds (or partly cloudy MODIS 10 km × 10 km boxes) with those away from clouds (or completely clear MODIS 10 km × 10 km boxes). We found that aerosol particles appear smaller near clouds in operational retrievals, as indicated by both the Ångström exponent and the SMAF, consistent with the results of *Loeb and Schuster* [2008]. After correction, averages of both the Ångström exponent and the SMAF become smaller near clouds than they are in regions away from clouds, suggesting larger aerosol particles near clouds as compared to regions away from clouds. This result is consistent with larger aerosols near clouds indicated by the color ratio from CALIPSO observations [e.g., *Tackett and Di Girolamo*, 2009; *Varnai and Marshak*, 2011].

[64] The algorithm applies to aerosol retrieval in the vicinity of clouds over the ocean. The current algorithm only applies to correct cloud-induced clear-sky enhancement due to the interaction between clouds and the molecular layer above. Our preliminary study found (not shown here) that 3-D cloud and ocean surface interaction can also lead to significant clear-sky reflectance enhancement in broken cloud fields over ocean. The enhancement due to this interaction

must be corrected for further improving the understanding of aerosol properties near clouds. It is also necessary to determine if the algorithm can be generalized to aerosol over land. Other factors such as remaining cloud contamination effects and indeterminate and variable combination of hydrated aerosol and subvisible cloud [e.g., *Charlson et al*., 2007] that may compensate bluing effects should be studied.

[65] Here we have to point out again that the two-layer model only corrects spectral radiances. The spectral AOD correction depends very much on the specifics of the MODIS aerosol retrieval algorithm. We are working on a research mode of the aerosol retrieval algorithm that will be more sensitive to the correction of spectral radiances.

[66] We have performed a detailed uncertainty analysis on reflectance correction and associated correction of aerosol properties. We found that the overall error in reflectance correction is about 10%, the error in AOD correction is about 1%, and the error in Ångström exponent correction is negligible.

[67] In the uncertainty analysis, we have considered only uncertainties due to errors in CERES flux and errors in input parameters in computing modeled fluxes. There are other sources that have not been examined in the present study. These sources include the error in the equal ratio assumption itself and unaccounted 3-D cloud and ocean surface and/or aerosol interactions. The simple method used to estimate flux for a MODIS $10\,\mathrm{km} \times 10\,\mathrm{km}$ box from flux for a larger CERES footprint also introduces errors in the flux estimate, consequently leading to errors in reflectance and aerosol corrections. Some of the errors in flux estimates due to mismatch between scenes taken from MODIS and CERES will cancel each other. However, the bias needs to be quantified. All these errors should be analyzed in a future study.

[68] The main sources of error in our correction model are assumptions such as the following: (i) molecular scattering dominates in the radiance enhancements at shorter wavelengths, (ii) aerosols are embedded in the boundary layer below cloud top, (iii) our models provide accurate narrowband-to-broadband flux ratios, etc. Each of these assumptions will be carefully tested in a future study using CALIPSO observations and cloud fields generated with large eddy simulations and Spherical Harmonic Discrete Ordinate Method simulations. We consider uncertainties in input parameters such as CERES broadband flux, cloud optical depth, cloud top height, and cloud fraction as secondary sources of error. The analysis of sensitivity is straightforward and will be carried out simultaneously with running the correction algorithm. These efforts will further help to improve understanding of aerosol properties near clouds.

[69] **Acknowledgments.** We gratefully acknowledge support for this research by the NASA Radiation Program managed by Hal Maring, the NASA CALIPSO project supervised by David Considine, and the NASA Terra/Aqua projects managed by Richard Eckman. We also thank Shana Mattoo for help with cloud mask analysis, as well as Anthony Davis, Rob Wood, and Mark Vaughan for insightful discussions and help.

References

Baum, B., W. P. Menzel, R. A. Frey, D. C. Tobin, R. E. Holz, and S. A. Ackerman (2012), MODIS cloud-top property refinements for Collection 6, *J. Appl. Meteor. Climatol.*, *51*, 1145–1163.

Cahalan, R. F., W. Ridgway, W. J. Wiscombe, T. L. Bell, and J. B. Snider (1994), The albedo of fractal stratocumulus clouds, *J. Atmos. Sci.*, *51*, 2434–2455.

Chakrapani, V., D. R. Doelling, and P. Minnis (2002), Conversion of narrowband visible radiances to broadband shortwave radiances using coincident CERES and VIRS data, 11th Conference on Atmospheric Radiation, Ogden, Utah, June 3–7.

Charlson, R. J., A. S. Ackerman, F. A.-M. Bender, T. L. Anderson, and Z. Liu (2007), On the climate forcing consequences of the albedo continuum between cloudy and clear air, *Tellus*, *59*, 715–727.

Geier, E. B., R. N. Green, D. P. Kratz, P. Minnis, W. F. Miller, S. K. Nolan, C. B. Franklin (2003), Single Satellite Footprint TOA/Surface Fluxes and Clouds (SSF) Collection Document.

Hansen, J. E., and L. Travis (1974), Light scattering in planetary atmosphere, *Space Sci. Rev.*, *16*, 527–610.

Ignatov, A., and L. Stowe (2000), Physical basis, premises and self-consistency checks of aerosol retrievals from TRMM VIRS, *J. Appl. Meteorol.*, *39*, 2259–2277.

Jeong, M. J., and Z. Li (2010), Separating real and apparent effects of cloud, humidity, and dynamics on aerosol optical thickness near cloud edges, *J. Geophys. Res.*, *115*, D00K32, doi:10.1029/2009JD013547.

Kaufman, Y. J., D. Tanré, L. A. Remer, E. F. Vermote, A. Chu, and B. N Holben (1997), Operational remote sensing of tropospheric aerosol over land from EOS moderate resolution imaging spectroradiometer, *J. Geophys. Res.*, 102, 17,051–17,067.

Kassianov, E. I., and M. Ovtchinnikov (2008), On reflectance ratios and aerosol optical depth retrieval in the presence of cumulus clouds, *Geophys. Res. Lett.*, *35*, L06807, doi:10.1029/2008GL033231.

King, M. D., Y. J. Kaufman, W. P. Menzel, and D. Tanré (1992), Remote sensing of cloud, aerosol, and water vapor properties from the Moderate Resolution Imaging Spectrometer (MODIS), *IEEE Trans. Geosci. Rem. Sens.*, *30*, 2–27.

King, M. D., W. P. Menzel, Y. J. Kaufman, D. Tanré, B.-C. Gao, S. Platnick, S. A. Ackerman, L. A. Remer, R. Pincus, and P. Hubandks (2003), Cloud and aerosol properties, precipitable water, and profiles of temperature and water vapor from MODIS, *IEEE Trans. Geosci. Rem. Sens.*, *41*, 442–458.

Koren, I., L. A. Remer, Y. J. Kaufman, Y. Rudich, and J. V. Martins (2007), On the twilight zone between clouds and aerosols, *Geophys. Res. Lett.*, *34*, L08805, doi:10.1029/2007GL029253.

Li, Z., and H. G. Leighton (1992), Narrowband to broadband conversion with spatially autocorrelated reflectance measurements, *J. Appl. Meteor.*, *31*, 412–432.

Loeb, N. G., and G. L. Schuster (2008), An observational study of the relationship between cloud, aerosol and meteorology in broken low-level cloud conditions, *J. Geophys. Res.*, *113*, D14214, doi:10.1029/2007JD009763.

Loeb, N. G., S. Kato, K. Loukachine, and N. Manalo-Smith (2005), Angular distribution models for top-of-atmosphere radiative flux estimation from the Clouds and the Earth's Radiant Energy System instrument on the Terra satellite. Part I: Methodology, *J. Atmos. Oceanic Technol.*, *22*, 338–351.

Loeb, N. G., W. Sun, W. F. Miller, K. Loukachine, and R. Davies (2006), Fusion of CERES, MISR, and MODIS measurements for top-of-atmosphere radiative flux validation, *J. Geophys. Res.*, *111*, D18209, doi:10.1029/2006JD007146.

Loeb, N. G., S. Kato, K. Loukachin, N. Manalo-Smith, and D. R. Doelling (2007), Angular distribution models for top-of-atmosphere radiative flux estimation from the Cloud and the Earth's Radiant Energy System Instrument on the Terra satellite. Part II: Validation, *J. Atmos. Oceanic Technol.*, *24*, 546–584.

Marshak, A., G. Wen, J. Coakley, L. Remer, N. G. Loeb, and R. F. Cahalan (2008), A simple model for the cloud adjacency effect and the apparent bluing of aerosols near clouds, *J. Geophys. Res.*, *113*, D14S17, doi:10.1029/2007JD009196.

Minnis, P., and E. F. Harrison (1984), Diurnal variability of regional cloud and clear-sky radiative parameters derived from GOES data; Part III: November 1978 radiative parameters, *J. Clim. Appl. Meteorol.*, *23*, 1032–1052.

Minnis, P., et al. (2011), CERES Edition-2 cloud property retrievals using TRMM VIRS and Terra and Aqua MODIS data—Part I: Algorithms, *IEEE Trans. Geosci. Remote Sens.*, *49*(11), 4373–4400.

O'Neill, N. T., T. F. Eck, B. N. Holben, A. Smirnov, and O. Dubovik (2001), Bimodal size distribution influences on the variation of Ångström derivatives in spectral and optical depth space, *J. Geophys. Res.*, *106*(D9), 9787–9806.

Platnick S., R. Pincus, B. Wind, M. D. King, M. A. Gray, and P. Hubanks (2004), An initial analysis of the pixel-level uncertainties in global MODIS cloud optical thickness and effective particle size retrievals, Proc. SPIE 5652, Passive Optical Remote Sensing of the Atmosphere and Clouds IV, 20, doi:10.1117/12.578353.

Redemann, J., Q. Zhang, P. B. Russell, J. M. Livingston, and L. A. Remer (2009), Case studies of aerosol remote sensing in the vicinity of clouds, *J. Geophys. Res.*, *114*, D06209, doi:10.1029/2008JD010774.

Remer, L. A., et al. (2005), The MODIS aerosol algorithm, products, and validation, *J. Atmos. Sci.*, *62*, 947–973.

Sanghavi, S. V., J. V. Martonchik, A. B. Davis, and D. D. Diner (2013), Linearization of a scalar matrix operator method radiative transfer model with respect to aerosol and surface properties, *J. Quant. Spectrosc. Radiat. Transf.*, *116*(2013), 1–16.

Schuster, G. L., O. Dubovik, and B. N. Holben (2006), Ångström exponent and bimodal aerosol size distributions, *J. Geophys. Res.*, *111*, D07207, doi:10.1029/2005JD006328.

Stamnes, K., S. C. Tsay, W. J. Wiscombe, and K. Jayaweera (1988), Numerically stable algorithm for discrete-ordinate-method radiative transfer in multiple scattering and emitting layered media, *Appl. Opt.*, *27*, 2502–2509.

Su, W., G. L. Schuster, N. G. Loeb, R. R. Rogers, R. A. Ferrare, C. A. Hostetler, J. W. Hair, and M. D. Obland (2008), Aerosol and cloud interaction observed from high spectral resolution lidar data, *J. Geophys. Res.*, *113*, D24202, doi:10.1029/2008JD010588.

Sun, W., N. G. Loeb, R. Davies, K. Loukachine, and W. F. Miller (2006), Comparison of MISR and CERES top-of-atmosphere albedo, *Geophys. Res. Lett.*, *33*, L23810, doi:10.1029/2006GL027958.

Tackett, J. L., and L. Di Girolamo (2009), Enhanced aerosol backscatter adjacent to tropical trade wind clouds revealed by satellite-based lidar, *Geophys. Res. Lett.*, *36*, L14804, doi:10.1029/2009GL039264.

Thomas, G. E., and K. Stamnes (1999), *Radiative Transfer in the Atmosphere and Ocean*, Cambridge University Press, New York.

Varnai, T., and A. Marshak (2011), Global CALIPSO observations of aerosol changes near clouds, *Geosci. Rem. Sens. Lett.*, *8*(*1*), 19–23 doi:10.1109/LGRS.2010.2049982.

Wagner, F., and A. M. Silva (2008), Some considerations about Ångström exponent distributions, *Atmos. Chem. Phys.*, *8*, 481–489.

Wen, G., A. Marshak, and R. F. Cahalan (2008), Importance of molecular Rayleigh scattering in the enhancement of clear sky radiance in the vicinity of boundary layer cumulus clouds, *J. Geophys. Res.*, *133*, D24207, doi:10.1029/2008JD010592.

Wielicki, B. A., B. R. Barkstrom, E. F. Harrison, R. B. Lee III, G. L. Smith, and J. E. Cooper (1996), Clouds and the Earth's radiant energy system (CERES): An Earth observing system experiment, *Bull. Amer. Meteorol. Soc.*, 77, 853–868.